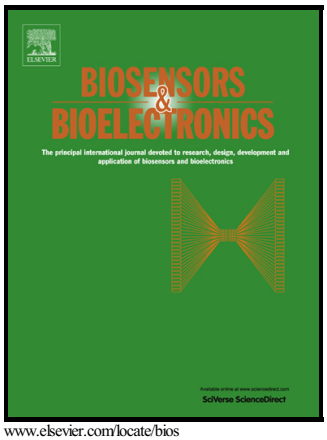


www.elsevier.com/locate/bios

# Selective nonenzymatic bilirubin detection in blood samples using a Nafion/Mn-Cu sensor

Hui-Bog Noh, Mi-Sook Won, Yoon-Bo Shim

PII: S0956-5663(14)00405-9
DOI: http://dx.doi.org/10.1016/j.bios.2014.06.002
Reference: BIOS6826

To appear in: *Biosensors and Bioelectronic*

Received date: 21 April 2014
Accepted date: 1 June 2014

Cite this article as: Hui-Bog Noh, Mi-Sook Won and Yoon-Bo Shim, Selective nonenzymatic bilirubin detection in blood samples using a Nafion/Mn-Cu sensor, *Biosensors and Bioelectronic,* http://dx.doi.org/10.1016/j.bios.2014.06.002

# Selective nonenzymatic bilirubin detection in blood samples using a Nafion/Mn-Cu sensor

Hui-Bog Noh [a], Mi-Sook Won [b], Yoon-Bo Shim [a,*]

[a] *Department of Chemistry and Institute of BioPhysio Sensor Technology (IBST), Pusan National University, Busan 609-735, South Korea.*

[b] *Busan Center, Korea Basic Science Institute (KBSI), Busan 609-735, South Korea*



[*] Corresponding author, Prof. Yoon-Bo Shim

Department of Chemistry and Institute of BioPhysio Sensor Technology (IBST),

Pusan National University, Busan 609-735, South Korea.

Tel.: +82-51-510-2244; Fax: +82-51-514-2122; E-mail: ybshim@pusan.ac.kr

**ABSTRACT**

The specific detection of biological organics without the use of an enzyme is challenging, and it is crucial for analytical and clinical chemistry. We report specific nonenzymatic bilirubin detection through the catalytic oxidation of bilirubin molecule on the Nafion/Mn-Cu surface. The catalytic ability, true surface area, morphology, crystallinity, composition, and oxidation state of the sensor surface were assessed using voltammetry, coulometry, XPS, XRD, Brunauer-Emmett-Teller (BET), SEM, EDXS, and TOF-SIMS experiments. The results showed that the surfacs was composed of microporous Mn-Cu bimetallic crystal in flake shape with a large BET surface area (3.635 $m^2 g^{-1}$), where the surface area and crystallity mainly affected the sensor performance. Product analysis of the catalytic reaction on the sensor probe revealed a specific two-electron oxidation of dipyrromethane moiety to dipyrromethene in the bilirubin molecule. Experimental variables affecting the analysis of bilirubin were optimized in terms of probe composition, temperature, pH, and potential. At the optimized condition, the dynamic range was between 1.2 μM and 0.42 mM, which yielded the equation of $\Delta I$ (μA) = (1.03 ± 0.72) + (457.0 ± 4.03) [C] (mM) with 0.999 of correlation coefficient, and the detection limit was 25.0 ± 1.8 nM ($n = 5$, $k = 3$). The stability test, interference effects, and analysis of real clinical samples, human whole blood and certified serum samples were demonstrated to confirm the reliability of the proposed bilirubin sensor.

**Highlights**

- We report specific nonenzymatic bilirubin detection using a Nafion/Mn-Cu sensor.
- The oxidation of bilirubin to biliverdin was confirmed by two-electron oxidation r eaction.
- The linear dynamic range of the sensor was between 1.2 μM and 0.42 mM (DL:

25.0 ± 1.8 nM).

- The sensor was successfully used for bilirubin detection in human whole blood and serum samples.

*Keywords:* Nafion/Mn-Cu sensor; Catalytic reaction mechanism; Amperometric biosensor; Nonenzymatic bilirubin sensor



## 1. Introduction

Bilirubin is a tetrapyrrole compound and the end product of heme from hemoglobin and myoglobin as well as many respiratory enzymes, including cytochromes (Sherlock, 1981; With, 1968). Approximately 6 g of hemoglobin is broken down daily, and 30 mg of bilirubin is formed. The production of bilirubin occurs in reticuloendothelial cells, particularly in the liver and spleen (Sherlock, 1981). Bilirubin is converted into urobilinogens by bacteria in the intestine, which are excreted partly in the urine. Hence, the bilirubin concentration can be used as an important guide to confirm liver function and to identify various liver diseases. The bilirubin level in normal adult serum ranges between $10^{-5}$ and $10^{-6}$ M (With, 1968). A high bilirubin level may cause serious disease, such as cirrhosis, jaundice, etc. (Hargreaves, 1968; Maisels, 1999). Otherwise, a low bilirubin level is related to coronary artery disease (Schiff and Schiff, 1993) and anemia (Kanada and Onishi, 1981). Thus, the analysis of bilirubin in body fluids is clinically important, which demands the development of an inexpensive and robust analytical method.

The conventional analytical method for bilirubin is UV-visible spectroscopy (Doumas et al., 1987; Bergmeyer, 1985). However, there are limitations to the method, such as interference from other heme proteins in the spectroscopic measurement (Doumas et al., 1973) and pH dependence in a diazo reaction (Li and Rosenzweig, 1997). Although electrochemical methods (Wang et al., 1985; Wang and Ozsoz, 1990), including voltammetry, polarography, and amperometry have also been developed, these are less selective than the diazo reaction. In addition, there have been many attempts including enzymatic reactions (Mullon and Langer, 1987; Kurosaka et al., 1998; Guo and Dong, 1997; Andreu et al., 2002) to achieve accuracy and selectivity for bilirubin detection. However, the use of enzymatic biosensors still has disadvantages, which are insufficient stability and irreproducibility due to the enzyme nature. Thus, the development of a stable and highly selective nonenzymatic sensor for bilirubin analysis is crucial.

To allow the specific detection of biologically important molecules without enzymes, one method is to prepare or identify a catalyst that can drive a specific reaction with target molecules. Of these catalysts, metals and metal oxides having a catalytic ability toward a specific reaction have received much attention to date (Fierro, 2005). However, extensive studies using metals or metal oxides have been focused on the catalytic reactions for energy conversion systems (Bochris and Khan, 1993). There are relatively few studies using metals for the catalytic reaction of organic and biological species for analytical purposes. The identification of new catalysts for the specific detection of biomolecules without enzymes is crucial. Bilirubin contains an active site moiety, dipyrromethane that is oxidized to form biliverdin. However, a nonenzymatic catalyst for the bilirubin oxidation had not yet been elucidated, although the oxidation of the dipyrromethane moiety to dipyrromethene has been performed with 2,3-dichloro-5,6-dicyano-1,4-benzoquinone (DDQ) and 2,3,5,6-tetrachlorocyclohexa-2,5-diene-1,4-dione (*p*-Chloranil) in various solvents at -78 °C (Groves

et al., 2013). Due to the extreme catalytic reaction conditions, they cannot catalyze the oxidation of the dipyrromethane moiety in the bilirubin structure in aqueous media and room temperature for further analytical applications. Thus, we attempted to identify a nonenzymatic catalyst for this oxidation. For the first time, we observed the oxidation of the dipyrromethane moiety in bilirubin using a Nafion/Mn-Cu sensor, which is a simple and efficient catalyst, at room temperature, and we applied this catalyst as a bilirubin sensor.

In the present study, certain metals expected to drive the catalytic oxidation of bilirubin were prepared electrochemically and tested for the selective oxidation of bilirubin. Coulometry, UV-visible spectrometry, electrospray ionization mass spectrometry (ESI-MS), cyclic voltammetry (CV), and linear sweep voltammetry (LSV) were used to evaluate the mechanism of catalytic oxidation of bilirubin and its analytical application. In addition, the characterization of a bimetallic catalyst was performed using various surface analysis methods, including X-ray photoelectron spectroscopy (XPS), X-ray diffractometry (XRD), Brunauer-Emmett-Teller (BET), scanning electron microscopy (SEM), energy dispersive X-ray spectroscopy (EDXS), and time-of-flight secondary ion mass spectrometry (TOF-SIMS). Experimental variables affecting the analysis of bilirubin were optimized and it was applied to real human whole blood and serum samples.



## 2. Experimental

### *2.1. Reagents and materials*

$CuCl_2$ (99.999%), $CoCl_2 \cdot 6H_2O$ (98%), $MnCl_2 \cdot 4H_2O$, $Na_2SO_4$, Nafion perfluorinated ion-exchange resin (5 wt.%), $NaH_2PO_4$, $Na_2HPO_4$, bilirubin, and certified serum sample were purchased from Sigma-Aldrich Chemical Co. (USA). The buffer solution was prepared using

$NaH_2PO_4$ + $Na_2HPO_4$ mixtures (PBS). The stock solution of bilirubin was prepared by dissolving 2.0 mg bilirubin in 0.1 mL of 0.1 M NaOH and diluted it with 6.0 mL of PBS (pH 8.0). The bilirubin measuring solution was diluted with stock solution daily before each experiment. Aqueous solutions were prepared with ultra-pure water obtained from a Milli-Q purifying system (18 MΩ cm). The glassy carbon (GC), Cu, Au, and Pt disk electrodes (3.0 mm diameter) were purchased from Kosentech (South Korea).

*2.2. Apparatus*

The electrodeposition of the sensing materials, along with coulometry, CV, LSV, and chronoamperometry were performed using a potentiostat (Kosentech Model KST-P1, South Korea). GC, Cu, Au, or Pt disk were used as working, Ag/AgCl (sat. KCl) as the reference, and Pt wire as counter electrodes, respectively. The XPS experiments were performed using a K-alpha XPS system (Thermo Fisher, UK) including a monochromatic Al Kα source with charge compensation (KBSI at Busan). XRD (X'pert PRO MRD system) was imployed to determine Mn-Cu bimetal crystallinity. SEM images and EDXS data were obtained using a Quanta 200 (FEI, USA) with a Schottky type thermal FE gun. The TOF-SIMS was TOF-SIMS 5 (ION TOF GmbH, Germany) with a bismuth liquid metal ion source. The UV-Visible spectra were obtained using a Cary 5000 spectrophotometer (Varian, USA), and the electrospray ionization-mass (ESI-MS) measurement was performed employing a HCT Basic System (Bruker, Germany). To confirmed performance of the sensor, standard bilirubin concentration in the samples was measured using a commercial bilirubin-monitoring meter from Green Cross Bio Science Lab., South Korea (Modular Analytics, Model-D, Germany).

*2.3. Preparation of the nonenzymatic Nafion/Mn-Cu sensor*

Prior to the preparation and electrochemical characterization of sensor probe, the electrodes for probe were polished with 0.5 μm alumina powder and cloth to a mirror finish, then rinsed them with distilled water. The electrochemical deposition of CoCu or Mn-Cu nanostructured metals on the electrode substrate was carried out in a 0.1 M $Na_2SO_4$ electrolyte solution containing 50.0 mM $CuCl_2$ and $CoCl_2{\cdot}6H_2O$, or $MnCl_2{\cdot}4H_2O$. The preparation conditions for these materials were optimized at first by varying the potentials at -1.00, -1.05, -1.10, and -1.15 V, and the resulting surfaces were evaluated with SEM (Supplementary material, Fig. S1). As the potential goes to more negative to -1.15 V, the current response is enhanced, but it remains unchanged over -1.15 V. In this case, nano-sized flake Mn-Cu microstructure is formed uniformly and densely on a Cu disk at -1.10 V. Hence, the optimum potential for a Mn-Cu bimetal was determined to be -1.10 V with an electrolysis time of 1000.0 s. The Mn-Cu electrode was covered with a 0.5% Nafion solution (10.0 μL) followed by rinse the surface with 0.1 M HCl, acetone, ethanol, and distilled water several times. Nafion coated Mn-Cu probe was dried in the $CaCl_2$ containing box at room temperature for 30 min before measurements.

*2.4. Real sample measurements*

The human whole blood was pretreated by centrifugation to get serum. In the centrifugation process, the plasma was separated from 2.0 mL of the whole blood by centrifugation at 3000 rpm for 10 min at 4 °C. The supernatant (serum) was collected for further experiments, and the pellet was discarded. The sample was diluted 5-fold with 0.1 M PBS (pH 7.0) for amperometry, and the standard serum sample was used for the parallel analysis.

## 3. Results and discussion

### *3.1. Voltammetric behaviors of the bilirubin oxidation on the nonenzymatic sensor*

The catalytic oxidation of bilirubin at single metal or bimetallic surfaces was investigated in aqueous media (~pH 7.0). Initially, the LSVs were recorded for Au, Pt, Co/Cu (Co was deposited on the Cu disk), CoCu/Cu (CoCu was deposited on the Cu disk), and Mn-Cu deposited surfaces. All of these probes showed oxidation peaks between approximately 0.0 and +0.40 V; however, no catalytic peak corresponding to bilirubin oxidation was observed, with the exception of the Mn, Cu, and Mn-Cu bimetallic surfaces. Among these, the Mn-Cu bimetallic surface clearly showed the selective catalytic oxidation process of bilirubin, which was applicable to nonenzymatic bilirubin detection. Thus, the catalytic abilities of these were evaluated in PBS containing 326.0 μM bilirubin. The CVs separately recorded for the Mn, Cu, and Mn-Cu surfaces showed the pairs of redox peaks at -0.03/+0.40 and -0.30/+0.04 V in PBS, corresponding to the redox couples of $Mn^{3+}/Mn^{4+}$ and $Cu^{+}/Cu^{2+}$ (not shown) from the metals themselves. As shown in Fig. 1(A), the PBS containing bilirubin showed an anodic peak at +0.39 V (*vs.* Ag/AgCl) corresponding to the bilirubin oxidation at the Cu surface, whereas no anodic peak appeared in the LSV recorded for the mere Cu in the blank solution. Otherwise, the mere Mn surface (Fig. 1(B)) had the much larger peak current for the bilirubin oxidation than that of the Cu at +0.32 V. The anodic peak current of the bilirubin oxidation on the Mn-Cu bimetallic surface (Fig. 1(C)) was 127.97 μA at +0.36 V, which was 35 and 13-fold higher than the response using pure Cu and Mn surfaces, respectively.

### *3.2. Characterization of the sensing probe material*

To identify the oxidation states of the bimetallic surfaces involved in the bilirubin oxidation, XPS analyses were performed before and after bilirubin oxidation (Fig. 2(A)). In this case, XPS spectra were obtained immediately after electrodeposition in a $N_2$-purged solution or after reactions, where samples were transferred into the XPS chamber under the vacuum condition. Fig. 2(A) shows XPS spectra for (a) $Mn2p_{3/2}$ and (b) $Cu2p_{3/2}$ after the experiments under different conditions as follows: the spectrum (I) was for the pure bimetallic electrode; (II) was for the electrode after the potential scanning from -0.70 to +0.30 V in PBS; (III) was for the electrode after the scanning from -0.15 to +0.80 V in PBS; and (IV) was for the electrode after the scanning from -0.70 to +0.80 V in 326.0 μM bilirubin containing PBS. As shown in the figure, spectrum (I) using the pure bimetallic electrode displayed peaks at 638.6 and 932.0 eV, corresponding to $Mn^0$ and $Cu^0$, respectively, in which both Mn and Cu exist entirely in the reduced metallic state. After the potential application to the bimetallic electrode at +0.30 V (II) in the blank solution, the intensities of the $Mn^{2+}$ (641.0 eV) and $Cu^+$ (932.5 eV) peaks increased significantly. When the potential increased to +0.80 V (III), the peak intensities of the $Mn^{3+}$ (641.4 eV), $Mn^{4+}$ (642.4 eV), and $Cu^{2+}$ (934.6 eV) ions were larger than those of $Mn^{2+}$ and $Cu^+$. The additional small peaks were also observed at approximately 645.6 - 647.1 eV (Mn) and 940.3 - 943.4 eV (Cu) due to the formation of $Mn^{2+}$, $Mn^{3+}$, and $Cu^{2+}$ (Oku et al., 1975; Marco et al., 2006; Stewart et al., 2004; Noh et al., 2012; Briggs and Seah, 1993). The $Mn^{2+}$, $Mn^{3+}$ (26%), and $Cu^+$ peak intensities in the spectra (IV) were higher than those of (III), which was after the bilirubin was oxidized at the Mn-Cu bimetallic electrode. This result indicates that $Mn^{3+}$, $Mn^{4+}$, and $Cu^{2+}$ are more closely related to the catalytic reaction of the bilirubin oxidation. In particular, the reaction related to the change in the oxidation state from $Mn^{4+}$ to $Mn^{3+}$ plays an important role in the catalytic oxidation of bilirubin (Briggs and Seah, 1993). Therefore, Mn ions contribute more significantly to the bilirubin oxidation in particular because Mn has various and high

oxidation states that can specifically interact with specific chemical bonds of organic species, such as the dipyrromethane moiety in the bilirubin structure.

To evaluate the sensor performance according to crystallinity of the probe material, the XRD spectra were obtained as a function of surface concentration, where the Mn ion concentration was varied from 10.0 to 100.0 mM. As shown in Fig. 2(B), four well-defined peaks appeared at 28, 44, 51, and 74 of $2\theta^{o}$, which indicated formation of Mn-Cu crystal (Mn (111) and Cu (111, 200, and 220)). Each peak of Mn-Cu is clearly distinguishable, representing that the bimetal crystals are grown successfully. The intensities of peaks corresponding to Cu decreased and Mn increased gradually with the increase in the concentration of Mn ion from 10.0 to 50.0 mM. However, the intensities of Cu and Mn peaks are unchanged over 50.0 mM concentration. XRD peaks of Mn (111) and Cu (111, 200, and 220) are identified as being body-centered cubic (bcc) of Mn and face-centered cubic (fcc) of Cu (Bondi et al., 2009; Qiu et al., 2009). The optimized concentration of Mn ions to show the highest crystallinity of Mn-Cu bimetal was 50.0 mM of Mn ions that reveals the best performance of the sensor. The crystallinity of Mn (111) and Cu (111) is closely related to the sensor performance that might be the most effective orientation for the bilirubin molecule adsorption, since the activity of the electrode surface is affected by the amount of adsorbate that depends on the size of adsorbing molecule and its orientation on the electrode surface (Bard and Faulkner, 2001). This result might be similar to the case of Au (111) single crystal surface that has the larger roughness factor compared with other crystal structure (Kim et al., 1992).

The (a) true surface area and (b) total pore volume of the nano-sized flake Mn-Cu structure was evaluated using their BET measurements as shown in Fig. 2(C). As the reaction proceeds, the crystals began to grow on the surface of Cu substrate. Compared with the surface area of bare Cu as 2.543 $m^2\ g^{-1}$, the values of prepared flaky structures with the Mn ion

concentrations of 10.0, 30.0, 50.0, 75.0, and 100.0 mM on Cu surface area were determined as 2.843, 3.024, 3.635, 3.621, and 3.619 $m^2 g^{-1}$, respectively (Fig. 2(C(a)). The maximum surface area was obtained at 50.0 Mm and no change was observed over 50.0 mM. It is worth noting that their morphologies at the different concentration of Mn ions are well matched with roughness value variation by BET measurement, and it is in confidence with the XRD result. Fig. 2(C(b)) shows total pore volume for Mn-Cu microstructure at different concentration of Mn ion. At 50.0 mM, the Mn-Cu film is densely formed with minimum total pore volume of 3.378 x $10^{-3}$ cc/g.

The morphologies of Mn-Cu bimetal probe revealed nano-flakes in SEM image, as shown in Fig. 2(D(a)). Mn deposited on the Cu surface had a similar structure to that of a carambola, an ornamental evergreen tree with a star-shaped ridged character (Briggs and Seah, 1993). At -1.10 V, with an electrolysis time of 1000.0 s, nanostructured Mn materials formed uniformly and densely on the Cu disk. As the potential went more negative than -1.05 V, bimetal in less dense was shown, which did not fully cover the surface of the Cu disk. In contrast, as the potential was more negative than -1.15 V, bimetal was formed in the significantly aggregated. To determine the content ratio of Mn to Cu in bimetal nano-flakes, the EDXS analysis was performed (Fig. 2(D(b))). When the potential applied at -1.10 V, the atomic content ratio of Mn:Cu was 55.8:44.2. To obtain further evidence for the distribution of Mn and Cu during nano-flake growth, TOF-SIMS images were acquired using in a positive mode. The analysis area was 5.0 x 5.0 $\mu m^2$. Fig. 2(E) shows of the Mn-Cu bimetal images in the mode of (a) $Cu_2^+$, (b) $Mn^+$, and (c) an overlay of $Cu_2^+$ (red) and $Mn^+$ (blue) ion components. Bright colors on the images corresponded to higher intensities of each species. $Cu_2^+$ and $Mn^+$ were chosen due to their clear signals. We can observe that Mn and Cu were very closely grown in an interlaced and complementary fashion. This homogeneous distribution of Mn and Cu in a

nano-flake structure indicates that the catalytic efficiency to the bilirubin oxidation is promoted more easily.

*3.3. Electrocatalytic oxidation of bilirubin on the Nafion/Mn-Cu electrode*

To evaluate the mechanism of bilirubin oxidation on the Nafion/Mn-Cu probe, the number of electrons participated in the oxidation process was at first determined by employing controlled potential coulometry, then the product was analyzed with UV-visible spectrometry and ESI-MS. The experiments were performed in a 5.0 mL blank solution (0.1 M PBS, pH 7.0) and a 1.0 μM bilirubin solution, separately. Electrolysis potential applied at +0.4 V (*vs.* Ag/AgCl) for 4000.0 s. In both cases, the charges were determined to be -15.05 and -16.02 mC for 4000.0 s each. The coulometric results revealed that bilirubin was oxidized primarily to a specified product by the participation of 2.01 electrons at the Nafion/Mn-Cu electrode.

To confirm the oxidized products of bilirubin at the Nafion/Mn-Cu electrode, we performed UV-visible and ESI-MS measurements both before and after bilirubin oxidation. As shown in Fig. 3(A), bilirubin has an absorption maximum near 430 nm. After bilirubin was oxidized, the maximum absorption band of the product shifted to 370 nm, and a new peak was observed at 660 nm. These wavelengths are characteristic of biliverdin (Moussa et al., 1988; Petrier et al., 1979), and the presence of this product was confirmed employing ESI-MS. The mass spectra of bilirubin were obtained as shown in Fig. 3(B) (a) bilirubin and (b) oxidized products. Before the bilirubin oxidation reaction, the base peak of m/z was 584, corresponding to the molecular weight of bilirubin. In addition, the peak of 607 was observed from the addition of Na contained in the PBS. The base peak for the oxidized products ranged from 2 to 582 m/z. The major product from the bilirubin oxidation at +0.40 V was biliverdin, with a yield of 80%, which was produced by a two-electron reaction. This result indicates

that the two electron oxidation of the dipyrromethane moiety to dipyrromethene in the bilirubin structure occurs on the Nafion/Mn-Cu electrode at room temperature (Fig. 3(C)). This is the first observation for the oxidation of the dipyrromethane moiety in bilirubin using an efficient catalyst at room temperature.

*3.4. Optimization of the analytical variables*

The experimental variables were optimized in terms of the Mn ion concentration for the electrode preparation, the pH of the sample solution, the oxidation potential, and the measuring temperature using a 326.0 μM bilirubin solution. The effect of the Mn ion concentration on the catalytic oxidation was investigated for the response of the bimetal probe (Fig. 4(A)). When the concentration of $MnCl_2$ changed from 10.0 to 100.0 mM, the maximum current was observed at 50.0 mM and the current response decreased over 50.0 mM due to excessive aggregation of the metal components. The catalytic peak current of bilirubin recorded for the Mn-Cu bimetal probe made of with 50.0 mM concentrations of $MnCl_2$ is 135.4 μA, which is 3.8 times higher than that of 10.0 mM concentrations of $MnCl_2$. Thus, 50.0 mM was selected as the optimum Mn ion concentration for subsequent experiments (Fig. S2). Fig. 4(B) shows the pH dependency of the media on the response current between 5.6 and 8.0. In this case, the current increased as the pH shifted from 5.6 to 7.0, then it decreased from pH 7.4 (Fig. 4(B)). The maximum response was observed at the pH of 7.0. The decrease of current over pH 7.0 might is attributed to the hydroxide formation of manganese or copper ions at the pH. Thus, the optimum pH was chosen as 7.0. The effect of applied potential on the bilirubin oxidation was also studied with chronoamperometry (Fig. 4(C)). In this study, the current increased as the applied potential went from +0.05 V to +0.50 V. The maximum response was observed at +0.40 V, and the application of the more positive

potential over +0.50 V resulted in no increase in the current. Thus, optimum potential at +0.40 V was used in the subsequent amperometric measurement. The effects of temperature on the bilirubin oxidation were studied between 10 and 60 °C (Fig. 4(D)). As shown in the figure, the oxidation current gradually increased as the temperature went from 10 to 35 °C. The current, however, decreased over 40 °C because the oxidation is related to the temperature-dependent activity of Mn (Rahman et al., 2008). However, the subsequent experiment was carried out at 35 °C with consideration of the biological condition of the bilirubin detection.

*3.5. Interference effects and the calibration plot*

To evaluate the interference effects on the sensor performance, the response current was measured in the presence of certain common interfering substances using the Mn-Cu probe. In the amperometric responses shown in Fig. 5(A), those for ascorbic acid, uric acid, dopamine, glutamic acid, and glucose were displayed between 7 and 0.4% of the bilirubin signal. Ascorbic acid showed the largest interference of 7%; however, the 0.5% Nafion layer-covered sensors completely removed the interference by ascorbic acid. This confirms that the present probe is a highly selective nonenzymatic sensor for bilirubin detection, and it can be expanded for use in the selective bilirubin analysis for medical diagnosis. Fig. 5(B) shows the current-time plot obtained for a Nafion/Mn-Cu senor with respect to the bilirubin concentration. The successive addition of bilirubin in the range of 1.2 μM to 0.42 mM was performed. In this case, the urrent quickly increased to a steady-state as the bilirubin solution was introduced ($t_{95}$ = 10 s). The inset of Fig. 5(B) shows the calibration plot for the bilirubin analysis. Under the optimized conditions, the linear range was 1.2 μM to 0.42 mM. The response according to the bilirubin concentration yielded the linear equation of ΔI (μA) =

(1.03 ± 0.72) + (457.0 ± 4.03) [C] (mM) with 0.999 of correlation coefficient. The detection limit was determined to be 25.0 ± 1.8 nM based on five repeated measurements (95% confidence level, $k = 3$, $n = 5$). The relative standard deviation (RSD) was 3.7% at a bilirubin concentration of 10.0 μM. It is significantly lower than in previous bilirubin biosensors (Wang and Ozsoz, 1990) and fiber optic biosensors (Li et al., 1996). Thus, the proposed biosensor makes the diagnosis of coronary artery disease (Schiff and Schiff, 1993) and anemia (Kanada and Onishi, 1981), in which the concentration of bilirubin is very low, and it is also useful for acute or chronic jaundice in the concentration higher than 30.0 μM.

*3.6. Stability of the nonenzymatic Nafion/Mn-Cu sensor*

When the sensor was stored at room temperature (in a vacuum) for a period of five months, the sensor retained more than 95.2% of its initial response. In addition, the stability of the sensor to multiple uses was evaluated using the same electrode repeatedly in the bilirubin solution. The sensor lost only 1.8% of the initial response after approximately 75 continuous measurements. The superior stability of the Nafion/Mn-Cu senor may be ascribed to the stable bimetallic crystal formation and Nafion layer. The senor was retained 85% of its initial response after continues using for three months.

*3.7. Real sample analysis*

To examine reliability of the method, it was used to perform a bilirubin assay with human whole blood and standard serum samples. The amperometric analysis of the bilirubin content in the samples was performed using the standard addition method in which the samples were diluted five times with PBS, followed the addition of varying volume of a standard bilirubin

solution (Fig. 5(C)). Where, the samples were obtained from five healthy volunteers and comparing the results with those of the standard serum sample (*n* = *6*). The concentrations of the bilirubin in the diluted samples were determined by repeating the experiment three times, which are 0.10 (± 0.01) - 0.21 (± 0.04) for the blood and 0.15 ± 0.01 mg/dL for the serum. Considering the dilution, the actual bilirubin contents in the blood and the serum samples were calculated to be 0.52 (± 0.02) - 1.05 (± 0.05) and 0.74 ± 0.02 mg/dL, respectively (Table 1). The results were compared with that from a commercial bilirubin meter using in a hospital, which showed similar values for bilirubin contents in the blood and standard serum samples of 0.5 - 1.0 and 0.6 - 0.7 mg/dL, respectively. The method was evaluated through the paired *t*-test, in which the calculated *t* value (1.22) was less than the critical *t* value (2.571) at a 95% confidence level (*n* = 6), indicating good agreement between the comparative results using the proposed sensor and the commercial bilirubin monitoring systems (listed in Table 1).

**4. Conclusions**

A nonezymatic Nafion/Mn-Cu senor was successfully developed for the analysis of bilirubin. The maximum true surface area of the fabricated sensor probe was determined to be 3.635 $m^2 g^{-1}$ by using BET anaysis, where the largest sensor performance was observed. The catalytic oxidation product of bilirubin formed on the senor was confirmed to be biliverdin (a 2-electron product). The oxidation of the dipyrromethane moiety to dipyrromethene in the bilirubin structure was observed on the sensor probe at room temperature. A calibration plot for bilirubin revealed the linear dynamic range between 1.2 μM and 0.42 mM with the detection limit of 25.0 ± 1.8 nM under the optimized experimental conditions. The proposed sensor elucidated good stability and a fast response time (<10 s). The bilirubin analysis with

the nonenzymatic sensor was successfully evaluated through the determination of the bilirubin concentration in human whole blood and serum samples.

**Acknowledgments**

This work was supported by the NRF grant funded by the MEST, South Korea (Grant No. 20100029128). We thank Prof. Young Soo Kang of Sogang University for BET expriments.

**Appendix A. Supplementary material**

Supplementary data associated with this article can be found in the online version at http://.

**References**

Andreu, Y., Ostra, M., Ubide, C., Galban, J., de Marcos, S., Castillo, J.R., 2002. Talanta 57, 343-353.

Bard, A.J., Faulkner, L.R., 2001. Electrochemical Methods: Fundamentals and Applications, John Willey & Sons, New York.

Bergmeyer, H.U., 1985. Methods of Enzymatic Analysis, VCH, Weinheim.

Bochris, J.O'M., Khan, S.U.M., 1993. Surface Electrochemistry, Plenum Press, New York.

Bondi, J.F., Oyler, K.D., Ke, X., Schiffer, P., Schaak, R.E., 2009. J. Am. Chem. Soc. 131, 9144-9145.

Briggs, D., Seah, M.P., 1993. Practical Surface Analysis, John Willey & Sons, New York.

Doumas, B.T., Perry, B., Jendrzejczak, B., Davis, L., 1987. Clin. Chem. 3, 1349-1353.

Doumas, B.T., Perry, B.W., Sasse, E.A., Straumfjord Jr., J.V., 1973. Clin. Chem. 19, 984-993.

Fierro, J.L.G., 2005. Metal Oxides: Chemistry and Applications, CRC Press, Boca Raton.

Groves, B.R., Crawford, S.M., Lundrigan, T., Matta, C.F., Sowlati-Hashjin, S., Thompson, A., 2013. Chem. Comm. 49, 816-818.

Guo, Y.Z., Dong, S.J., 1997. Anal. Chem. 69, 1904-1908.

Hargreaves, T., 1968. The Liver and Bile Metabolism, Appleton-Century-Crofts, New York.

Kanada, N., Onishi, S., 1981. Biochem. J. 196, 257-260.

Kim,Y.-T., McCarley, R.L., Bard, A.J., 1992. J. Phys. Chem. 96, 7416-7421.

Kurosaka, K., Senba, S., Tsubota, H., Kondo, H., 1998. Clin. Chim. Acta 269, 125-136.

Li, X., Fortuney, A., Guilbault, G.G., Suleiman, A.A., 1996. Anal. Lett. 29, 171-180.

Li, X., Rosenzweig, Z., 1997. Anal. Chem. Acta 353, 263-273.

Maisels, M.J., 1999. Neonatology, Pathophysiology and Management of the Newborn, J. B. Lippincott Publisher, Philadelphia.

Marco, J.F., Gancedo, J.R., Nguyen-Gong, H., del Ganto, M., Gautier, J.L., 2006. Solid State Ion. 177, 1381-1388.

Moussa, F.M., Kanoute, G., Herrenknecht, C., Levillain, P., Trivin, F. 1988. Anal. Chem. 60, 1179-1185.

Mullon, C.J., Langer, R., 1987. Clin. Chem. 33, 1822-1825.

Noh, H.-B., Lee, K.-S., Chandra, P., Won, M.-S., Shim, Y.-B., 2012. Electrochim. Acta 61, 36-43.

Oku, M., Hirokawa, K., Ikeda, S.J., 1975. Electron. Spectrosc. Relat. Phenom. 6, 451-458.

Petrier, C., Dupuy, C., Jardon, P., Gautron, R., 1979. Photochem. Photobiol. 29, 389-392.

Qiu, R., Cha, H.G., Noh, H.-B., Shim, Y.-B., Zhang, X.L., Qiao, R., Zhang, D., Kim, Y.I., Pal, U., Kang, Y.S., 2009. J. Phys. Chem. C 113, 15891-15896.

Rahman, Md.A., Lee, K.-S., Park, D.-S., Won, M.-S., Shim, Y.-B., 2008. Biosens. Bioelectron. 23, 857-864.

Schiff, L., Schiff, E.R., 1993. Diseases of the Liver, Lippincott Publisher, Philadelphia.

Sherlock, S., 1981. Diseases of the Liver and Biliary System, Blackwell Scientific Publications, London.

Stewart, S.J., Multigner, M., Marco, J.F., Berry, F.J., Hernando, A., Gonzalez, J.M., 2004. Solid State Commun. 130, 247-251.

Wang, J., Luo, D.B., Farias, P.A.M., 1985. J. Electroanal. Chem. 185, 61-71.

Wang, J., Ozsoz, M., 1990. Electroanalysis 2, 647-650.

With, T.K., 1968. Bile Pigments, Chemical Biological and Clinical Aspects, Academic Press, New York.

**Figure captions**

**Fig. 1.** LSVs recorded for (A) bare Cu, (B) Mn/GC, and (C) Mn-Cu electrodes in 0.1 M PBS (pH 7.0, dotted line) and PBS containing 326.0 μM bilirubin (black solid line).

**Fig. 2.** (A) XPS spectra of the (a) $Mn2p_{3/2}$ and (b) $Cu2p_{3/2}$ peaks for the Mn-Cu bimetallic probe ((I) electrodeposition using the potential sweep between (II) -0.70 - +0.30 V or (III) -0.15 - +0.80 V in PBS (pH 7.0), and (IV) bilirubin oxidation). (B) XRD spectra of Mn-Cu bimetallic surface having different Mn ion concentration (10.0, 30.0, 50.0, 75.0, and 100.0 mM). (C) (a) Nitrogen adsorption-desorption isotherm curves and (b) total pore volume of Mn-Cu crystal structure depending on different Mn ion concentrations (0.0, 10.0, 30.0, 50.0, 75.0, and 100.0 mM). (D) (a) SEM image and (b) EDXS spectrum of Mn-Cu bimetallic probe. (E) TOF-SIMS images of the Mn-Cu bimetallic surface in (a) $Cu_2^+$, (b) $Mn^+$, and (c) a two-color overlay of $Cu_2^+$ (red) and $Mn^+$ (blue) ions. The field of view is 5.0 x 5.0 $\mu m^2$.

**Fig. 3.** (A) UV-visible spectra for bilirubin (black line) and the oxidized product of bilirubin (gray line). (B) ESI-MS results for (a) bilirubin and (b) the oxidized products. (C) The reaction scheme of the oxidation of the dipyrromethane moiety to dipyrromethene at the Nafion/Mn-Cu senor at room temperature.

**Fig. 4.** Optimization of the experimental variables: (A) the $Mn^{2+}$ concentration for the probe preparation, (B) the pH of the sample solution, (C) the applied potential, and (D) the temperature for the oxidation of bilirubin in 0.1 M PBS (pH 7.0) containing 326.0 μM bilirubin.

**Fig. 5.** (A) The chronoamperomeric responses for the interference effects of other bio-compounds with the Mn-Cu bimetallic probe. (B) The chronoamperometric responses observed at the Nafion/Mn-Cu senor after a successive injection of bilirubin (applied potential: +0.40 V) into the measuring solution. Inset: A calibration plot for the bilirubin detection under the optimized conditions. (C) Calibration plots using the standard addition method for the analysis of bilirubin in human blood and standard serum samples, respectively.

**Table 1.** A result of parallel bilirubin analysis of the whole blood and standard serum samples by the proposed sensor and the comparative analytical method.

| Samples | | Bilirubin concentration (mg/dL) | | | |
|---|---|---|---|---|---|
| | | Proposed method | Mean (SD) | Comparative method* | Mean (SD) |
| Human whole blood | No. 1 | 0.72<br>0.70<br>0.74 | 0.72 (± 0.02) | 0.7<br>0.7<br>0.6 | 0.67 (± 0.06) |
| | No. 2 | 1.05<br>1.01<br>1.10 | 1.05 (± 0.5) | 1.0<br>0.9<br>1.0 | 0.97 (± 0.06) |
| | No. 3 | 0.56<br>0.58<br>0.60 | 0.58 (± 0.02) | 0.6<br>0.6<br>0.6 | 0.60 (± 0.00) |
| | No. 4 | 0.62<br>0.61<br>0.65 | 0.63 (± 0.02) | 0.6<br>0.5<br>0.6 | 0.57 (± 0.06) |
| | No. 5 | 0.54<br>0.52<br>0.50 | 0.52 (± 0.02) | 0.5<br>0.6<br>0.5 | 0.53 (± 0.06) |
| Standard serum | No. 1 | 0.73<br>0.75<br>0.76 | 0.74 (± 0.02) | 0.6<br>0.7<br>0.7 | 0.67 (± 0.06) |

* Green Cross Bio Science Lab., South Korea (Modular Analytics, Model-D, Germany)

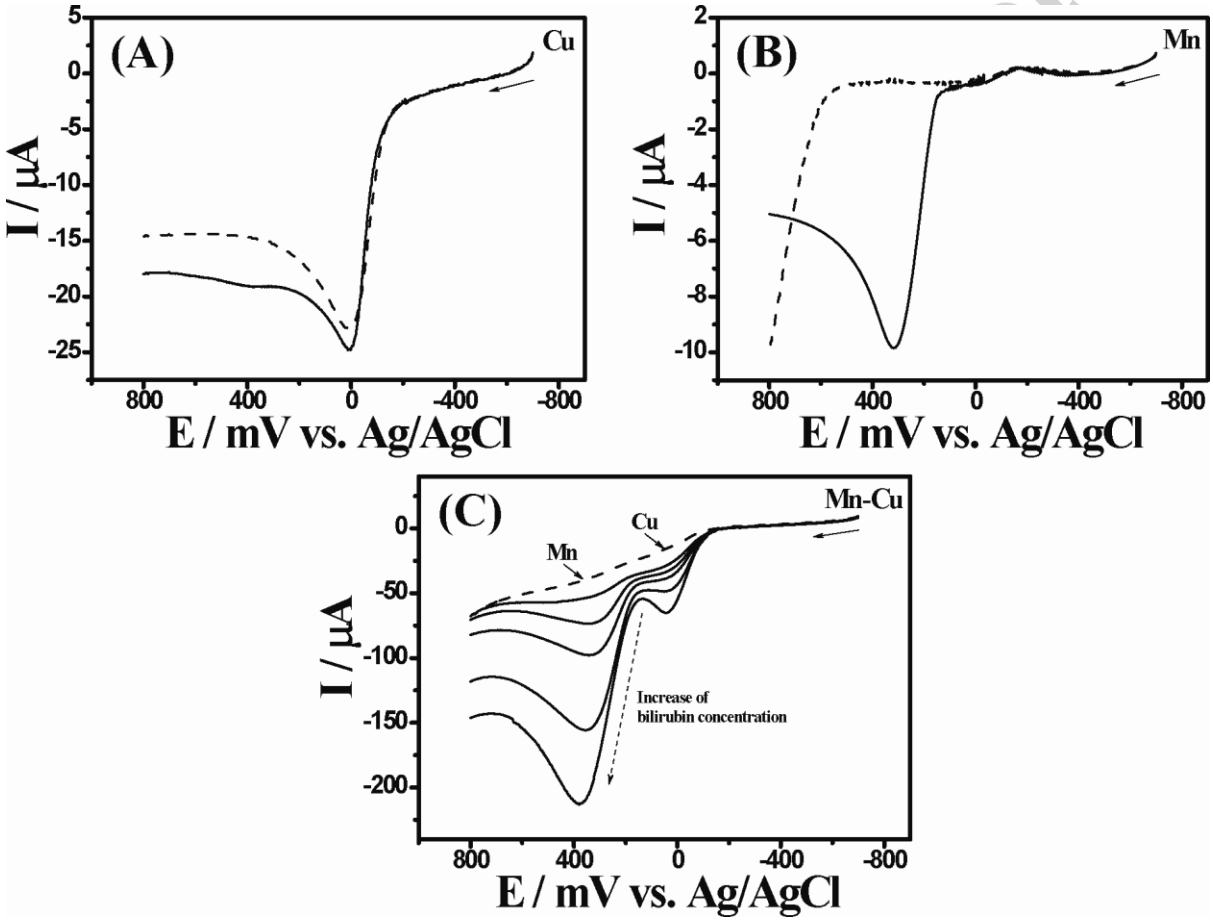
(A)
Cu
I / μA
E / mV vs. Ag/AgCl
(B)
Mn
I / μA
E / mV vs. Ag/AgCl
(C)
Mn-Cu
Cu
Mn
Increase of
bilirubin concentration
I / μA
E / mV vs. Ag/AgCl

**Fig. 1.**

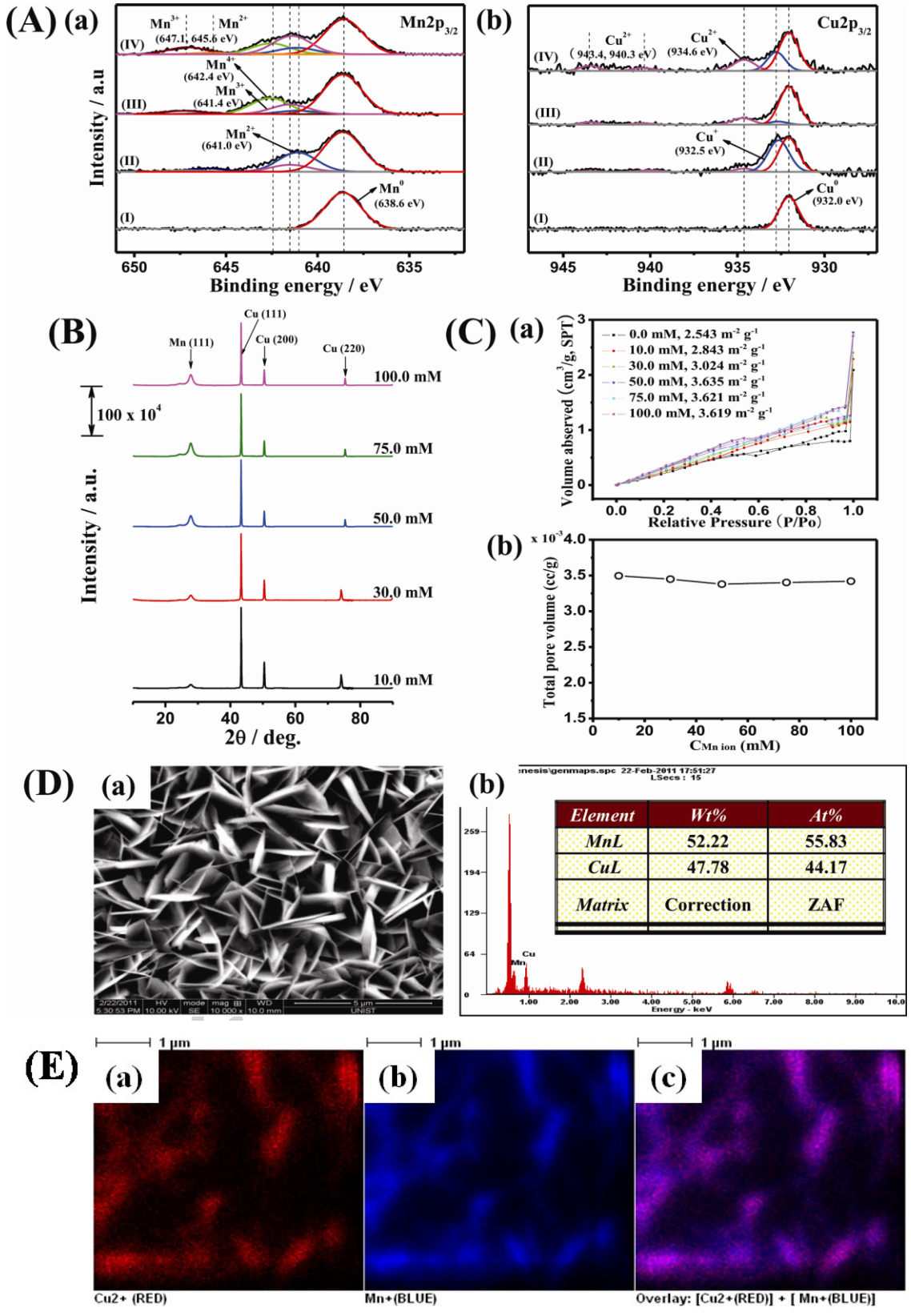
(A) (a)
Mn2p3/2
Mn3+ (647.1 eV)
Mn2+ (645.6 eV)
Mn4+ (642.4 eV)
Mn3+ (641.4 eV)
Mn2+ (641.0 eV)
Mn0 (638.6 eV)
(IV)
(III)
(II)
(I)
Intensity / a.u
Binding energy / eV
(b)
Cu2p3/2
Cu2+ (943.4, 940.3 eV)
Cu2+ (934.6 eV)
Cu+ (932.5 eV)
Cu0 (932.0 eV)
(B)
Mn (111)
Cu (111)
Cu (200)
Cu (220)
100.0 mM
75.0 mM
50.0 mM
30.0 mM
10.0 mM
100 x 10^4
Intensity / a.u.
2θ / deg.
(C) (a)
0.0 mM, 2.543 m2 g-1
10.0 mM, 2.843 m2 g-1
30.0 mM, 3.024 m2 g-1
50.0 mM, 3.635 m2 g-1
75.0 mM, 3.621 m2 g-1
100.0 mM, 3.619 m2 g-1
Volume observed (cm3/g, SPT)
Relative Pressure (P/Po)
(b)
x 10-3
Total pore volume (cc/g)
CMn ion (mM)
(D) (a)
(b)
Element | Wt% | At%
MnL | 52.22 | 55.83
CuL | 47.78 | 44.17
Matrix | Correction | ZAF
Cu
Mn
Energy - keV
(E)
(a)
(b)
(c)
1 μm
Cu2+ (RED)
Mn+(BLUE)
Overlay: [Cu2+(RED)] + [ Mn+(BLUE)]

**Fig. 2.**

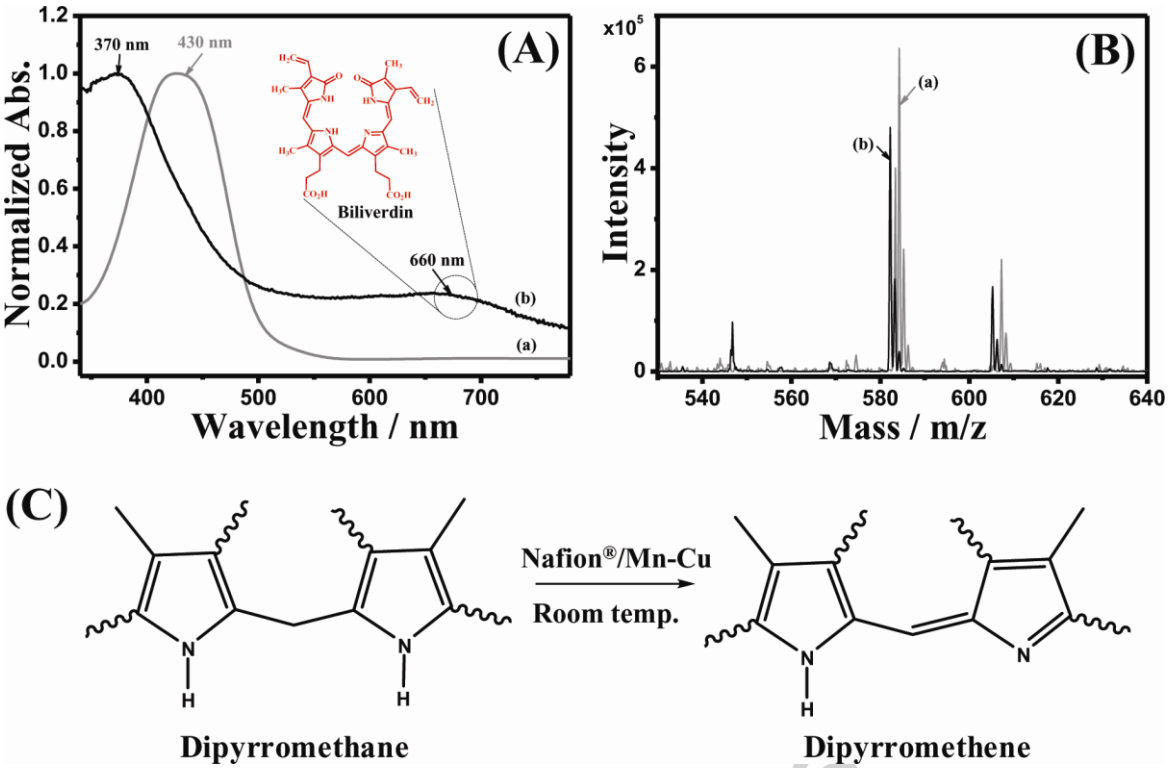


**Fig. 3.**

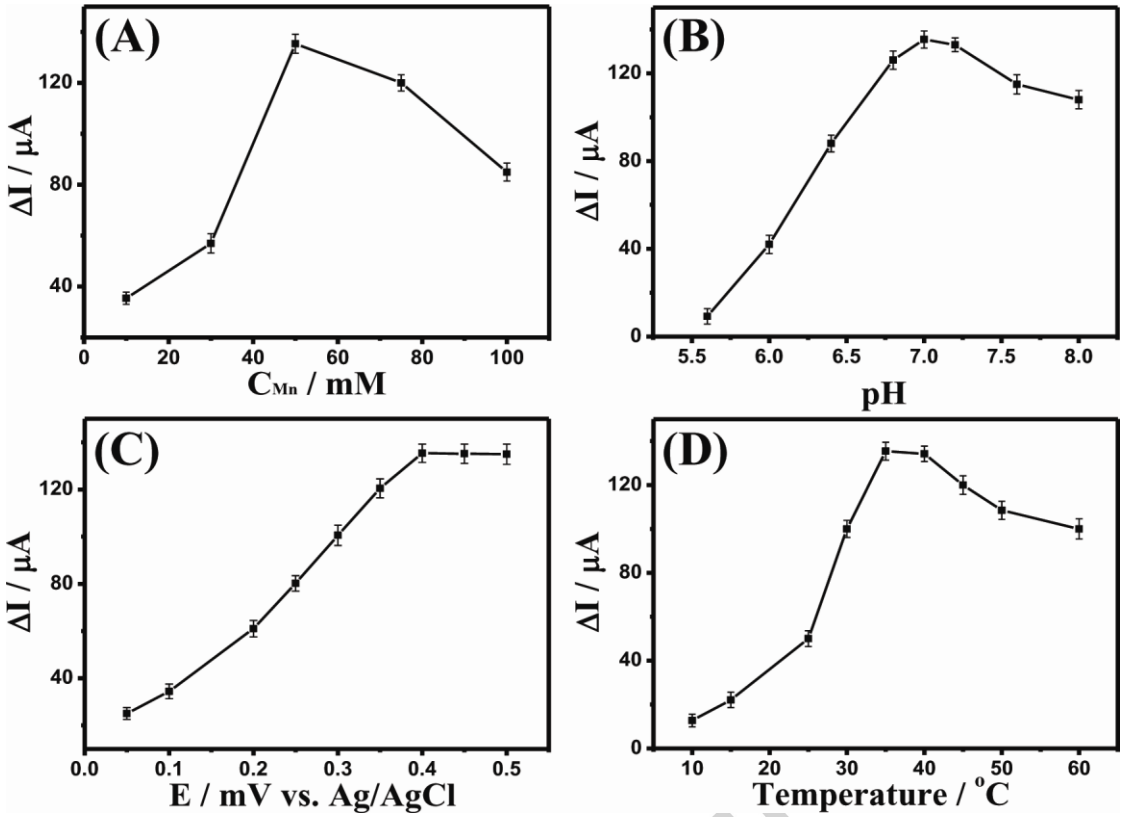


**Fig. 4.**

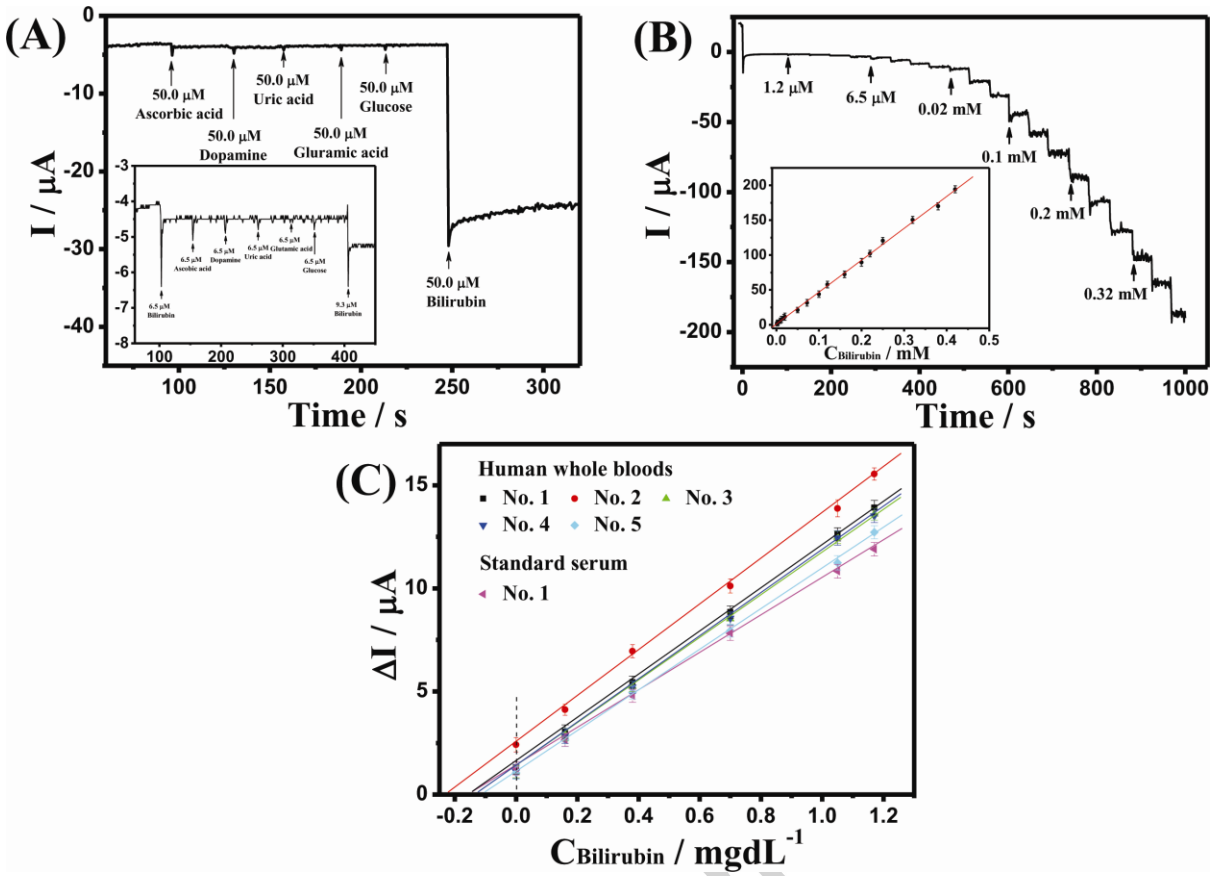


**Fig. 5.**